

Figure S1

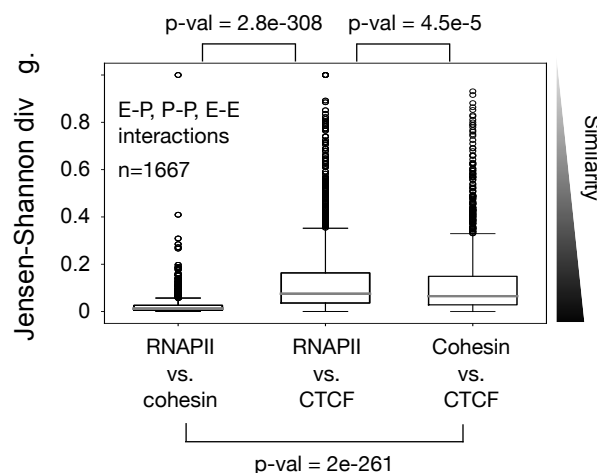
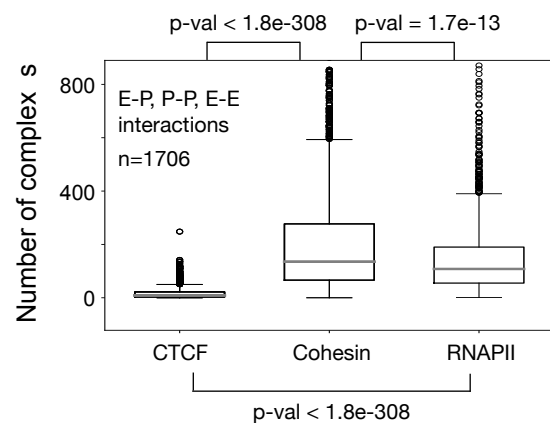
A

# of frag / complex	CTCF ChIA-Drop	%	Cohesin ChIA-Drop	%	RNAPII ChIA-Drop	%
2 F/C	1,371,547	88.1	8,840,000	86.6	2,075,177	86.5
3 F/C	132,181	8.5	953,873	9.3	228,709	9.5
4 F/C	31,166	2.0	244,566	2.4	57,608	2.4
5 F/C	10,794	0.7	90,060	0.9	19,815	0.8
≥6 F/C	11,357	0.7	82,819	0.8	18,424	0.8
Total # of chromatin complexes	1,557,045		10,211,318		2,399,732	

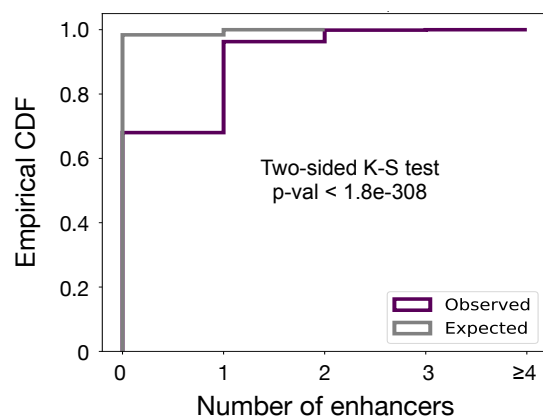
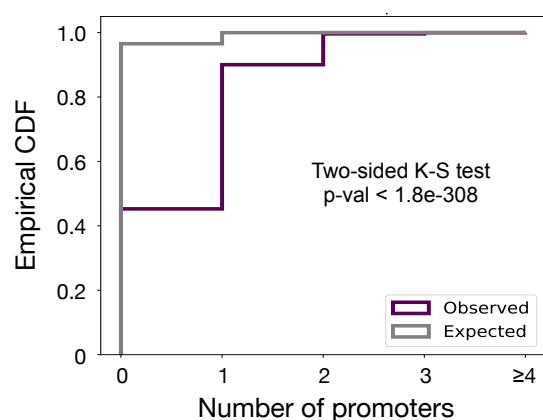
B

Data 1	vs.	Data 2	SCC
GM12878 cells			
CTCF ChIA-Drop Rep 1		CTCF ChIA-Drop Rep 2	0.81
CTCF ChIA-Drop Rep 1		CTCF ChIA-Drop Rep 3	0.78
CTCF ChIA-Drop Rep 2		CTCF ChIA-Drop Rep 3	0.78
CTCF ChIA-Drop		CTCF ChIA-PET	0.87
SMC1A ChIA-Drop		RAD21 ChIA-Drop Rep 1	0.75
SMC1A ChIA-Drop		RAD21 ChIA-Drop Rep 2	0.74
RAD21 ChIA-Drop Rep 1		RAD21 ChIA-Drop Rep 2	0.87
Cohesin ChIA-Drop		Cohesin ChIA-PET	0.72
RNAPII ChIA-Drop Rep 1		RNAPII ChIA-Drop Rep 2	0.76
RNAPII ChIA-Drop		RNAPII ChIA-PET	0.85

C



D



Promoters in RNAPII ChIA-Drop data

# of promoters / complex	Expected	%	Observed	%
0 promoter	2,316,500	96.5	1,086,441	45.2
1 promoter	82,282	3.4	1,073,944	44.8
2 promoter	941	0.04	229,688	9.6
3 promoter	8	0	8,695	0.36
≥4 promoter	1	0	964	0.04

Enhancers in RNAPII ChIA-Drop data

# of enhancers / complex	Expected	%	Observed	%
0 enhancer	1,069,072	98.4	738,877	68.0
1 enhancer	17,282	1.6	307,255	28.3
2 enhancer	87	0	38,854	3.6
3 enhancer	0	0	1,339	0.12
≥4 enhancer	0	0	116	0.01

Figure S1: ChIA-Drop data for mapping chromatin interactions mediated by CTCF, cohesin, and RNAPII.

(A) A table of ChIP-enriched CTCF, cohesin, and RNA Polymerase II (RNAPII) ChIA-Drop chromatin complexes by the number of fragments per complex (F/C). **(B)** Stratum-adjusted correlation coefficients (SCC) between all datasets of ChIP-enriched CTCF, RAD21, SMC1A, and RNAPII ChIA-Drop experiments and their replicates. R1, R2, and R3 denote replicates 1, 2, or 3 of a given experiment, respectively. SCC between ChIP-enriched ChIA-Drop and corresponding ChIA-PET data are also computed. **(C)** Boxplots for quantifications of transcriptional chromatin interactions. Left panel: number of chromatin complexes in CTCF, cohesin, and RNAPII ChIA-Drop data at 1,706 loop loci characterized in **Figure 1D**. Right panel: the Jensen-Shannon divergence of pairs of the datasets between RNAPII, cohesin, and CTCF ChIA-Drop (see **Methods**). p-values are computed from the two-sided Mann-Whitney U test. **(D)** Left panel: empirical cumulative distribution function (ECDF) of the observed (purple) and expected (grey) number of RNAPII ChIA-Drop complexes with 0, 1, 2, 3, and ≥ 4 promoters (top) and those with 0, 1, 2, 3, and ≥ 4 enhancers (bottom) are plotted. Right panel: the numbers and percentages of RNAPII ChIA-Drop complexes with promoters (top) and enhancers (bottom) that were expected and observed.

Figure S2

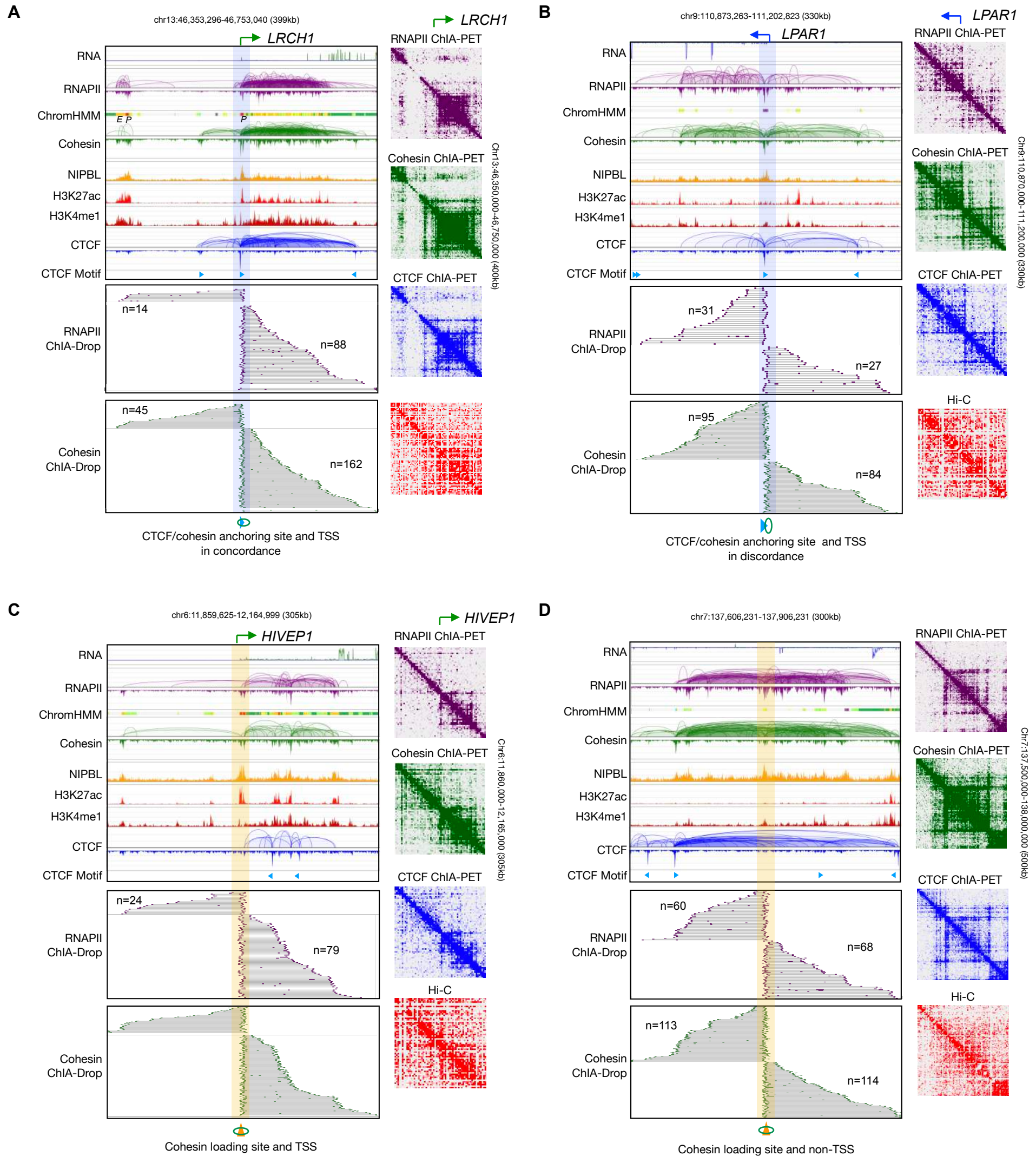


Figure S2: Transcriptional loops mediated by RNAPII and cohesin through concerted efforts.

(A) RNAPII binding site coinciding with the TSS of *LRCH1* at CTCF/cohesin anchoring site (highlighted in blue) in concordance with CTCF binding motif. Data tracks are RNA-seq, RNAPII ChIA-PET loops/peaks along with chromHMM states, cohesin ChIA-PET loops/peaks, NIPBL ChIP-seq, H3K27ac ChIP-seq, H3K4me1 ChIP-seq, CTCF ChIA-PET loops/peaks, and CTCF binding motifs, followed by the sorted views of RNAPII and cohesin ChIA-Drop complexes centered at the TSS. The 2D contact maps of RNAPII ChIA-PET, cohesin ChIA-PET, CTCF ChIA-PET, and Hi-C are accompanied on the right. (B) Similar to panel A, but at the TSS of *LPAR1* in discordance with CTCF/cohesin anchoring site. (C) Similar to panel A, but presenting RNAPII binding site and TSS of *HIVEP1* at NIPBL binding/cohesin loading site (highlighted in yellow). (D) Similar to panel A, but at the NIPBL binding/cohesin loading site not overlapping with TSS of any gene.

Figure S3

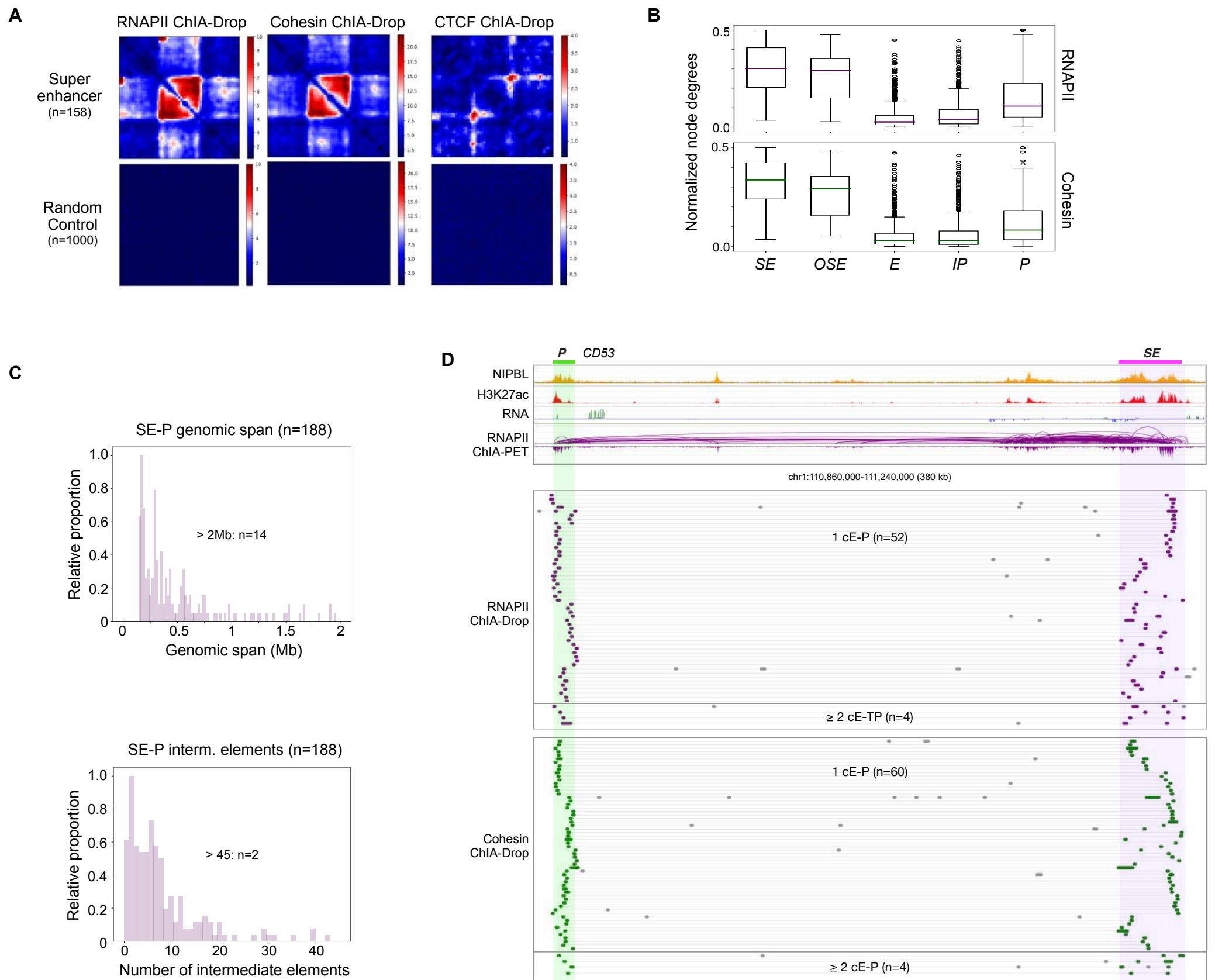


Figure S3: Multiplex transcriptional chromatin interactions involving super-enhancers.

(A) Aggregation of 2D pairwise contacts of RNAPII, cohesin, and CTCF ChIA-Drop data at super-enhancer regions and at random regions as negative controls. **(B)** Boxplots of normalized node degrees of SEs, other SE along the path (*OSE*), enhancers (*E*), intermediary promoters (*IP*), and target gene promoters (*P*) are plotted for the 188 SE-P pairs in RNAPII and cohesin ChIA-Drop data. **(C)** A histogram of genomic span of 188 SE-P structures, of which 14 are larger than 2 Mb (top). The number of intermediate elements between SE and P are also plotted (bottom). **(D)** An example of SE-P interactions at the *CD53* gene locus. Top tracks are ChIP-seq of NIPBL and H3K27ac, RNA-seq, and RNAPII ChIA-PET. Below are the fragment views of RNAPII (purple) and cohesin (green) ChIA-Drop complexes showing single-molecule resolution of SE-*CD53* interactions involving one constituent enhancer (1 cE-P) and multiple constituent enhancer (≥ 2 cE-P), where n denotes the number of chromatin complexes.

Figure S4

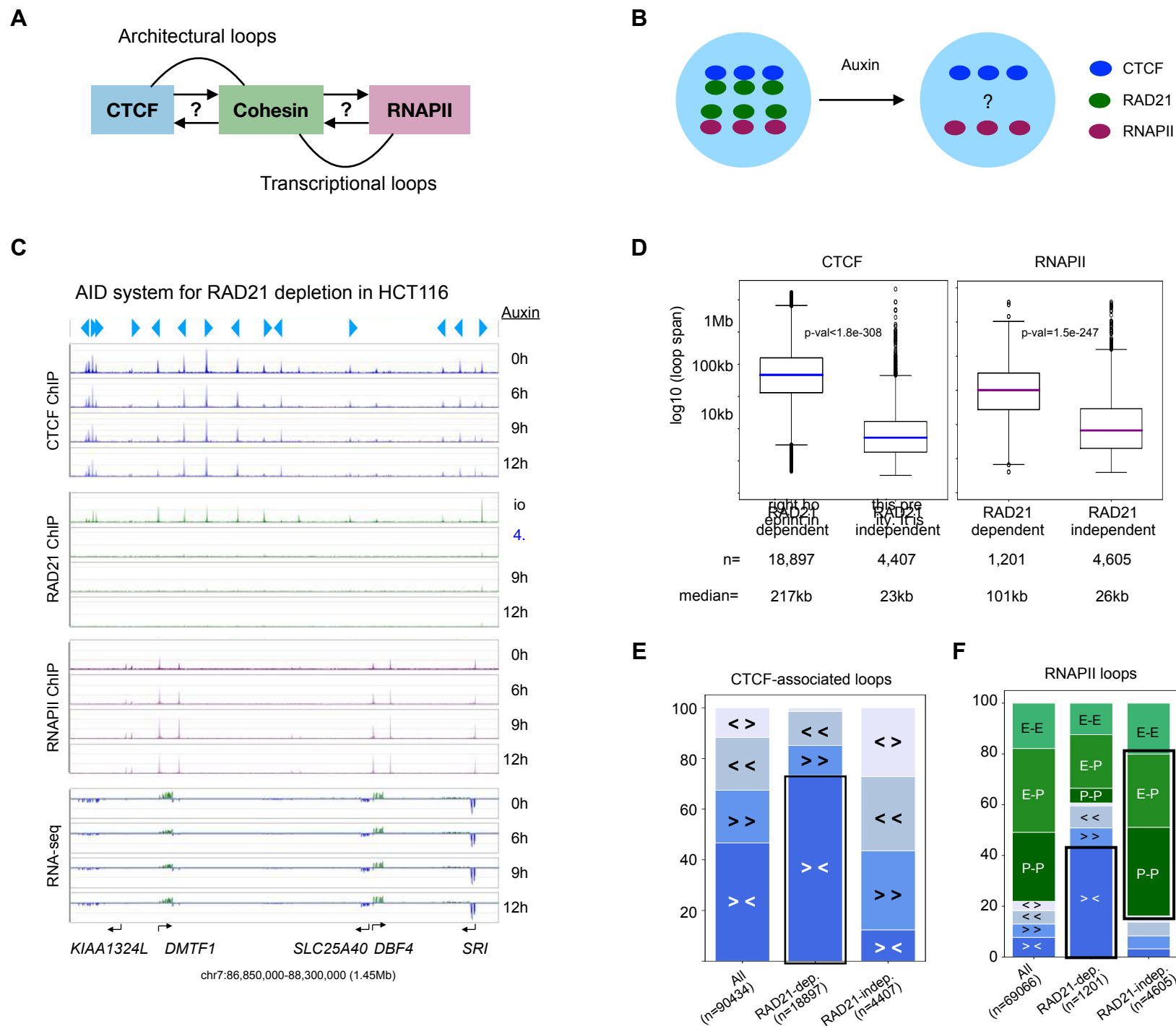


Figure S4: Effects of RAD21 depletion on long- and short-range chromatin interactions mediated by CTCF and RNAPII.

(A) A diagram questioning the causal roles of cohesin in forming architectural loops with CTCF and transcriptional loops with RNAPII. (B) A schematic of the Auxin Inducible Degron (AID) tagged cell line HCT116-RAD21-mAC for auxin (IAA)-inducible degradation of RAD21, a subunit of cohesin. (C) An example browser view of ChIP-seq data of CTCF, RAD21, and RNAPII and RNA-seq data in HCT116 cells tagged with Auxin-inducible Degron AID (HCT116-RAD21-mAC) with auxin (IAA) treatment for 0, 6, 9, and 12 hours. Light blue arrows indicate CTCF binding motif and orientations. (D) Boxplots of chromatin loop span in the categories of 'RAD21-dependent' (i.e., reduced loop strengths) and 'RAD21-independent' (unchanged) loops in CTCF and RNAPII ChIA-PET data (see **Methods**), where n denotes the number of loops in each category and median loop span recorded below. p-values are from the two-sided Mann-Whitney U test. (E) Segmented bar charts for the proportions of CTCF-associated chromatin loops in 'All', 'RAD21-dependent', and 'RAD21-independent' HCT116 loops. CTCF loops with binding motifs in 4 categories: convergent ('> <'), right tandem ('> >'), left tandem ('< <'), divergent ('< >'). (F) Segmented bar charts for the proportions of RNAPII-associated chromatin loops in 'All', 'RAD21-dependent', and 'RAD21-independent' HCT116 loops. RNAPII loops are first characterized by CTCF binding motifs as convergent ('> <'), right tandem ('> >'), left tandem ('< <'), divergent ('< >'), and the rest of the CTCF-free loops are further categorized as promoter-promoter ('P-P'), enhancer-promoter ('E-P'), and enhancer-enhancer ('E-E') loops.

Figure S5

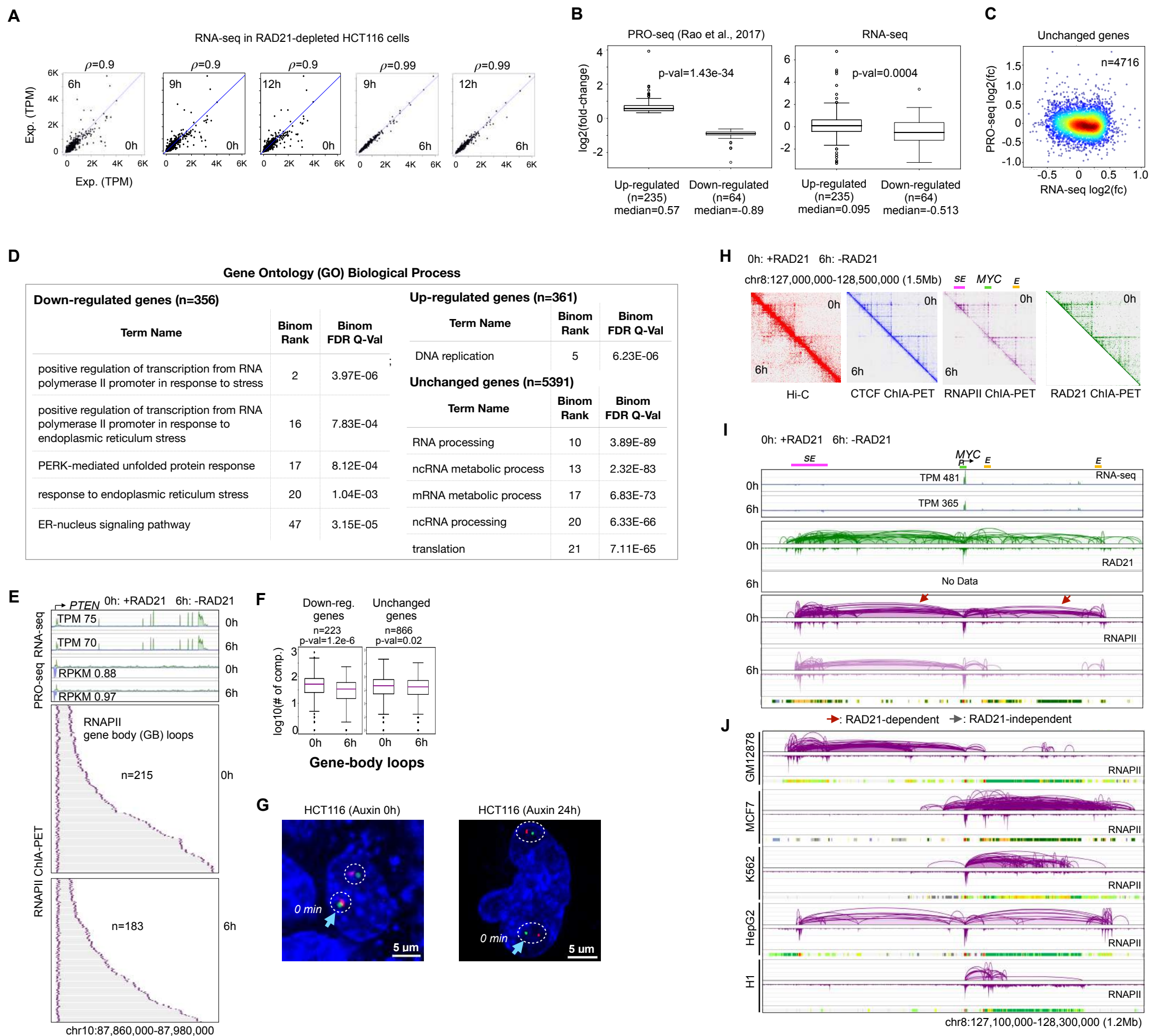


Figure S5: Functional roles of RAD21-dependent super-enhancer to promoter loop in transcription.

(A) Scatter plots of TPM (transcripts per kilobase million) of genes from RNA-seq with various timepoints of auxin treatment. ρ : Pearson's correlation coefficient. (B) Boxplots of log2(fold-change) of gene expression before and after depleting RAD21 of up-regulated and down-regulated genes from PRO-seq (left) and RNA-seq (right) datasets; up-regulated and down-regulated genes were defined by PRO-seq (Rao et al., 2017). (C) A scatterplot of log2(fold-change) of gene expression between RNA-seq and PRO-seq data for unchanged genes, with colors denoting the density of data points. (D) Gene Ontology terms enriched in down-regulated, up-regulated, and unchanged genes. (E) Gene body loops of RNAPII ChIA-PET data before (0h; h: hours) and after (6h) depleting RAD21 are sorted from the promoter of an unchanged *PTEN* gene towards the transcription end site in the same forward orientation as the gene transcription; n denotes the number of chromatin complexes. TPM (transcript per kilobase million) from RNA-seq (this study) and RPKM (reads per kilobase million) from PRO-seq (Rao et al., 2017) are also recorded. (F) Boxplots of log10 of number of complexes in the gene-body loops before (0h) and after (6h) depleting RAD21, plotted separately for down-regulated genes and unchanged genes. (G) Representative Casilio images of SOX9-SE loop anchors (two pairs of probes in circles per nucleus) in control HCT116-RAD21-mAC cells (Auxin 0h) and cells with 24 hours of auxin treatment for RAD21-degradation (Auxin 24h). The pair with light blue arrow in each image is further tracked in Figure 5G. Scale bars, 5 μm. (H) 2D contact maps of data before (0h) and after (6h) depleting RAD21 at a 1.5 Mb region centered around *MYC* gene, super-enhancer (SE) and enhancer (E) mapped via Hi-C, CTCF ChIA-PET, RNAPII ChIA-PET, and RAD21 ChIA-PET. Only 0h data exist for RAD21 ChIA-PET. (I) In a large chromatin domain (1.2 Mb) harboring *MYC* gene and associated regulatory elements super-enhancer (SE), enhancers (E) and promoter (P) demarcated by ChromHMM, tracks of RNA-seq, cohesin ChIA-PET, and RNAPII ChIA-PET loops/peaks in HCT116 cell line before (0h) and after (6h) depleting RAD21 are shown. TPM: transcripts per kilobase million. Reduced loops are marked by red arrows. (J) In the same region as panel I, the RNAPII ChIA-PET loops and peaks and chromHMM states are also shown for 5 other cell lines: GM12878, MCF7, K562, HepG2, H1.

Figure S6

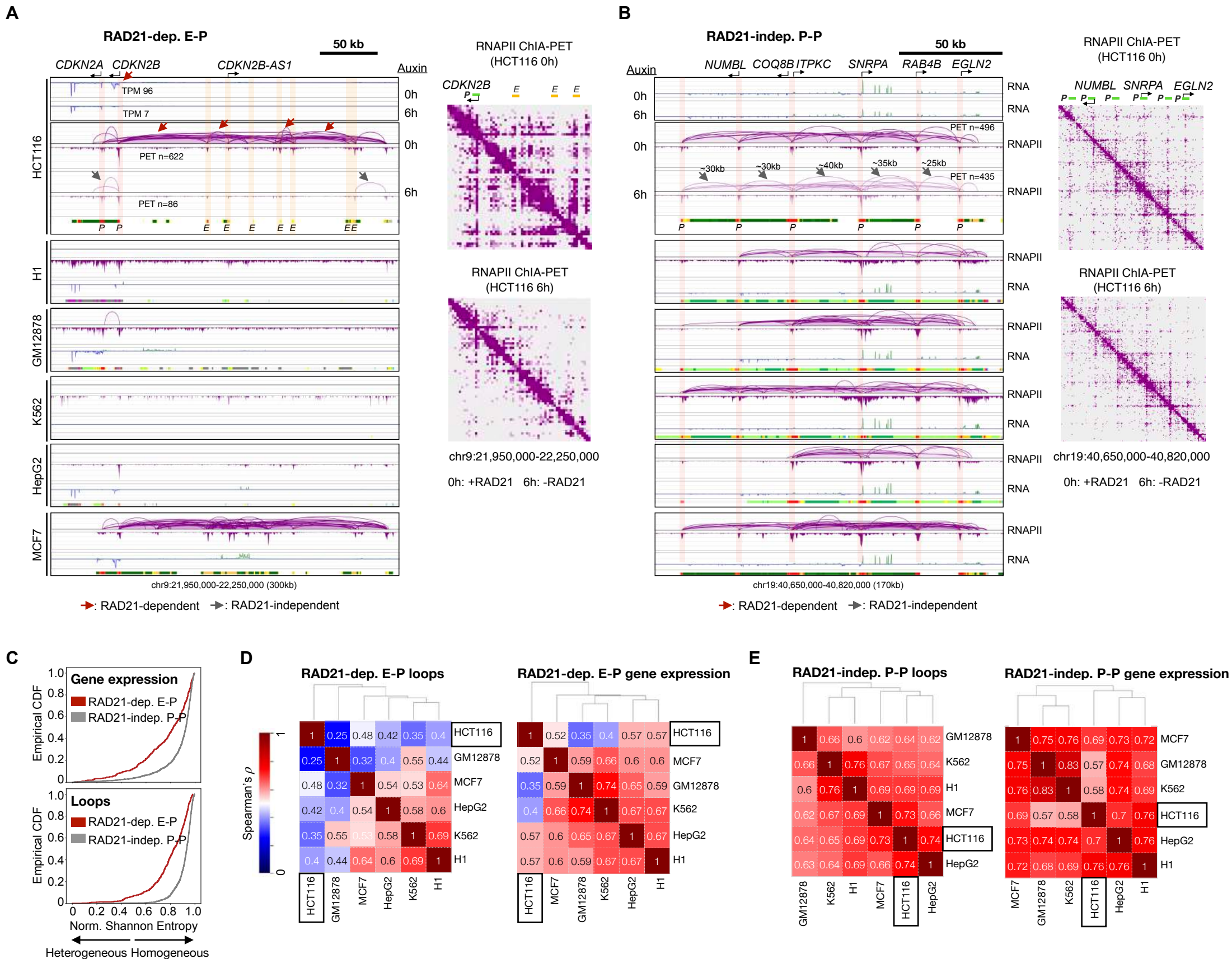


Figure S6: Distinct roles of RAD21-dependent E-P and RAD21-independent P-P RNAPII loops in gene regulation.

(A) A 300 kb region including a down-regulated *CDKN2B* gene, where RNAPII ChIA-PET, RNA-seq, and ChomHMM chromatin states are shown for HCT116 and 5 other cell lines: H1, GM12878, K562, HepG2, and MCF7. 2D contact maps of RNAPII ChIA-PET in HCT116 cells before (0h) and after (6h) RAD21 depletion are also shown. (B) A 170 kb region encompasses RAD21-independent RNAPII loops connecting promoters (P) of active genes. Annotations are consistent with those in panel A. (C) An empirical cumulative distribution function (CDF) of the normalized Shannon entropy (see **Methods**) quantified over 6 cell lines gene expression (top panel) and chromatin interaction strengths (bottom panel) involved in RAD21-dependent enhancer-promoter (E-P) and RAD21-independent promoter-promoter (P-P) loops. (D) The Spearman's correlation coefficient between the genomic profiles between all pairs of 6 cell lines, clustered via hierarchical clustering (see **Methods**). The left panel characterizes loop strengths of RAD21-dependent enhancer-promoter (E-P) loops and the right panel includes genes involved in these loops. (E) A similar plot as panel H for the RAD21-independent promoter-promoter (P-P) interactions and associated genes therein.

Figure 7: DNA replication signal patterns in differential genes, and proposed model.

(A) The median replication signal of gene body is plotted for each of the 16-stage Repli-seq data before (0 hour) and after (6 hour) depleting RAD21 for up-regulated, down-regulated, and unchanged genes, along with 20000 random regions (see **Methods**). **(B)** An up-regulated gene *CCNE1* with TPM (transcript per kilobase million) computed from RNA-seq data before (0h: 0 hour) and after (6h: 6 hours) depleting RAD21. A larger 3.15 Mb region encompassing *CCNE1* is shown with 16-stage Repli-seq data (Emerson et al., 2022) from early P02 to late P17 replication stages with auxin treatment denoting cell with (0h) or without (6h) RAD21. Red bar indicates the early initiation zone defined by Emerson et al. using HCT116 0h Repli-seq data. **(C)** Similar to panel **B**, for a down-regulated gene *OSBPL6*. **(D)** Chronologically, cohesin first loads to chromatin at NIPBL binding sites that are usually co-localized with RNAPII and active transcriptional elements (promoters, enhancers), then it goes along with RNAPII in the direction of transcription and establish short-range transcriptional interactions for local constitutive genes (P-P and E-P) and in long-range loops for connecting distal (super-)enhancers to target gene promoters (SE-P); after arriving at CTCF binding sites, cohesin is interlocked with CTCF, anchors itself there, and actively reels in DNA string in accordance with the CTCF motif orientation, thereby constituting large architectural loops. The architectural loops (blue), the long-range transcriptional loops (purple for RNAPII), and the associated genes are sensitive to RAD21 depletion (cohesin-dependent), whereas the short-range transcription loops (purple for RNAPII) and associated genes are cohesin-independent. See also **Figure S7**.

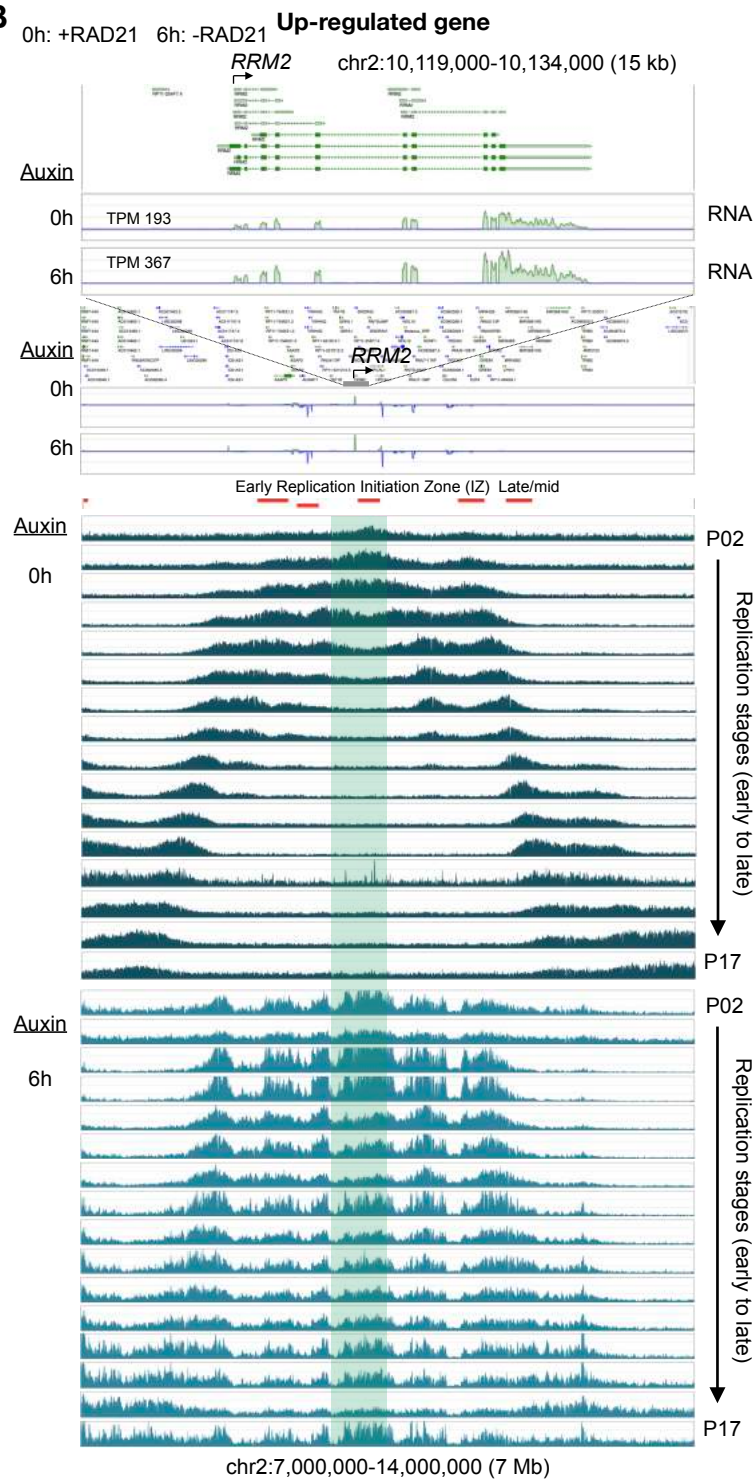
Figure S7

A

Up-regulated genes associated with DNA replication term in Gene Ontology

Gene Name	Description	Gene Name	Description
<i>ORC1</i>	Origin recognition complex subunit 1	<i>RRM2</i>	Ribonucleoside-diphosphate reductase subunit M2
<i>FAM111B</i>	Serine protease FAM111B	<i>DSCC1</i>	Sister chromatid cohesion protein DCC1
<i>GINS1</i>	DNA replication complex GINS protein PSF1	<i>FEN1</i>	Flap endonuclease 1
<i>CCNE2</i>	G1/S-specific cyclin-E2	<i>MCM10</i>	Protein MCM10 homolog
<i>CCNE1</i>	G1/S-specific cyclin-E1	<i>PCNA</i>	Proliferating cell nuclear antigen
<i>TOPBP1</i>	DNA topoisomerase 2-binding protein 1	<i>CHAF1A</i>	Chromatin assembly factor 1 subunit A
<i>GINS2</i>	DNA replication complex GINS protein PSF2	<i>GRWD1</i>	Glutamate-rich WD repeat-containing protein 1

B



C

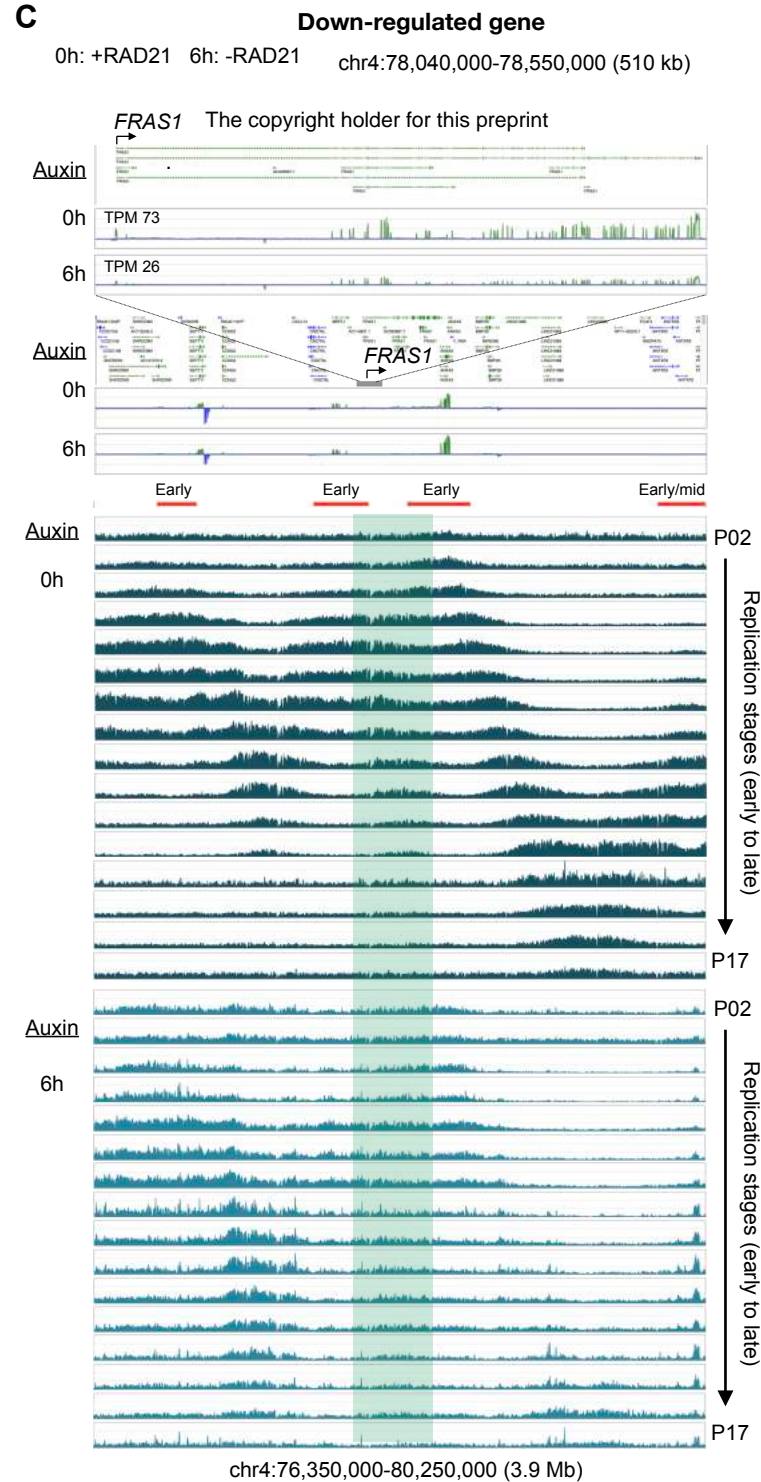


Figure S7: DNA replication signal patterns in differential genes, and proposed model.

(A) A list of 14 genes identified to be associated with DNA replication in Gene Ontology of up-regulated genes, along with their descriptions of functions. (B) An example of an up-regulated gene *RRM2* along with RNA-seq signal (top panel) and 16-stage Repli-seq (Emerson et al., 2022) signal from early P02 to late P17 stages in HCT116 cells before (0h; middle panel) and after (6h; bottom panel) RAD21 depletion. Red bars are replication initiation zones identified using 0h data in Emerson et al. with specific labels early or late/mid replication. (C) Similar to panel B, but for a down-regulated *FRAS1* gene.